**ARTICLE**

# Peritectic orthopyroxene entrainment during partial melting of garnet peridotite produced the Bushveld Complex chromite deposits

Tahnee Otto[1] · Gary Stevens[1] · Jean-François Moyen[2] · Matthew J Mayne[1] · John D Clemens[1]

## Abstract

One of the largest chromium deposits on Earth occurs in the Rustenburg Layered Suite (RLS) of the Bushveld Complex as laterally continuous chromitite layers. None of the hypotheses proposed for the origin of the chromitites can explain both the abundance of Cr in the RLS and the unusual enrichment in Cr and V over Ni, relative to typical depleted mantle values. This study investigates the possibility that the layering and chromitite formation are consequences of the entrainment of source components into the magmas that formed the RLS. Thermodynamic modelling results reveal a wedge-shaped domain in pressure-temperature space in the subcratonic mantle within which Cr-bearing orthopyroxene forms as a peritectic product of incongruent melting. Entrainment of this orthopyroxene produces magmas that crystallise peritectic olivine and chromite on ascent, due to the consumption of orthopyroxene by melt. The chromite- and olivine-bearing magmas intrude as sills and can produce chromite and dunite layers by density separation. This model, which interprets the RLS Sr-isotopic composition to reflect prior mantle metasomatism by crustal fluids (ideally ancient and of low volume), readily explains the formation of chromitite layers from relatively thin sills, as well as the very high ratios of Cr and V to other compatible elements relative to typical mantle compositions. The special circumstances required to produce the RLS chromitites do not relate to some oddity of repetitive crustal assimilation or magma compositions that allow chromite-only saturation. Rather, they relate to speed of melting and magma extraction which enabled peritectic orthopyroxene entrainment to the magmas.

**Keywords** Chromitites · Thermodynamic modelling · Peritectic · Mantle melting · Rustenburg Layered Suite · Bushveld Complex

## Introduction

The Rustenburg Layered Suite (RLS) of the Bushveld Complex, South Africa, is a giant ultramafic-mafic layered complex that contains most of Earth's viable chromium (Cr) and platinum reserves (Naldrett et al. 2009), suggesting its formation by potentially unique processes. Accounting for the vast amount of Cr in the RLS is a considerable challenge (e.g., Eales 2000). Possibly the most plausible mechanism proposed to date is that the RLS represents cumulates of basaltic-andesitic melts formed by assimilation of Kaapvaal craton crust by komatiite magmas (e.g., Eales and Costin 2012). Recent versions of this model also propose that the suite's layered rocks formed by multiple injections of crystal-slurry sills (Yao et al. 2021). However, the precipitation of chromite as a direct consequence of assimilation (Yao et al. 2021) means that each magma batch, following appreciable assimilation of the crust, must travel rapidly from the deep crustal site of assimilation to the upper crustal intrusion without losing the denser crystals along the way. Consequently, such a model requires that the high concentration of highly compatible elements in the mantle and in komatiites, which have very low abundances in crustal rocks, should be present in proportions within the average lower RLS that mirror their komatiitic roots. This does not appear to be so for two of the most important elements, Cr and Ni,

✉ Tahnee Otto
tahneeotto@sun.ac.za

[1] Earth Science Department, Stellenbosch University, Private Bag X1, Stellenbosch 7602, South Africa

[2] Laboratoire Magmas et Volcans, Université Jean Monnet, UCA-CNRS-IRD, Saint-Étienne, France

🙋 Springer

with most of the common silicate rocks of the Lower- and Critical Zones massively enriched in Cr over typical komatiite compositions and primitive mantle values (Fig. 1). In addition, the Sr-isotopic heterogeneity inherent to the RLS (Kruger 1994) poses an additional challenge to this hybridised magma model. Komatiitic magmas are unlikely to arise through the partial melting of mantle metasomatised by crustally derived fluids or melts because such metasomatised mantle is enriched in pyroxene (e.g., Keleman et al. 1998; Simon et al. 2007). Thus, if derived from hybridised komatiitic magmas, the recorded variable Sr-isotopic composition of the RLS can only be ascribed to assimilating variable amounts of crust, or crust of different compositions. In this study, we consider the Sr-isotopic variations in the RLS to reflect different magma batches sourced from isotopically variable mantle that was metasomatised by the addition of small amounts of crustally derived fluid or melt, possibly as much as 1 Ga prior to the formation of the RLS, during assembly of the craton.

By modelling the stoichiometries of partial melting reactions in garnet peridotite that may have produced the RLS parental magmas, an alternative hypothesis for the origin of RLS chromitites and its ferromagnesian layering is explored. In mantle source rocks, melting is incongruent; the melt has a composition different to the sum of the reactants. This must result in the formation of new, peritectic, crystalline phases (e.g., Grove et al. 2013; Kinzler 1997),

and their production at a variety of melt fractions provides ample opportunity for their entrainment into the magmas on segregation from the source. To this end, thermodynamically constrained petrological modelling was utilised to explore the effects of peritectic crystal entrainment on the chemistry of the resultant magmas (i.e., melt plus crystals) and their subsequent crystallisation in the upper crust. The results suggest a double-peritectic process, involving entrainment of peritectic orthopyroxene in the source and the reaction of this to produce peritectic olivine and chromite in the ascending magma. This process represents a highly efficient mechanism to explain the origin of RLS chromitites, and also fits well with Cr/Ni ratios of the RLS.

## Methods

### Modelling overview

There are three steps involved in the modelling method designed to investigate the details of melting reactions in mantle source rocks, the magma compositions that would result, and the partial crystallisation of these magmas in the upper crust. Details of each step are described fully in the sections below.

First, we studied the stoichiometry of the partial melting reactions in representative peridotitic mantle sources
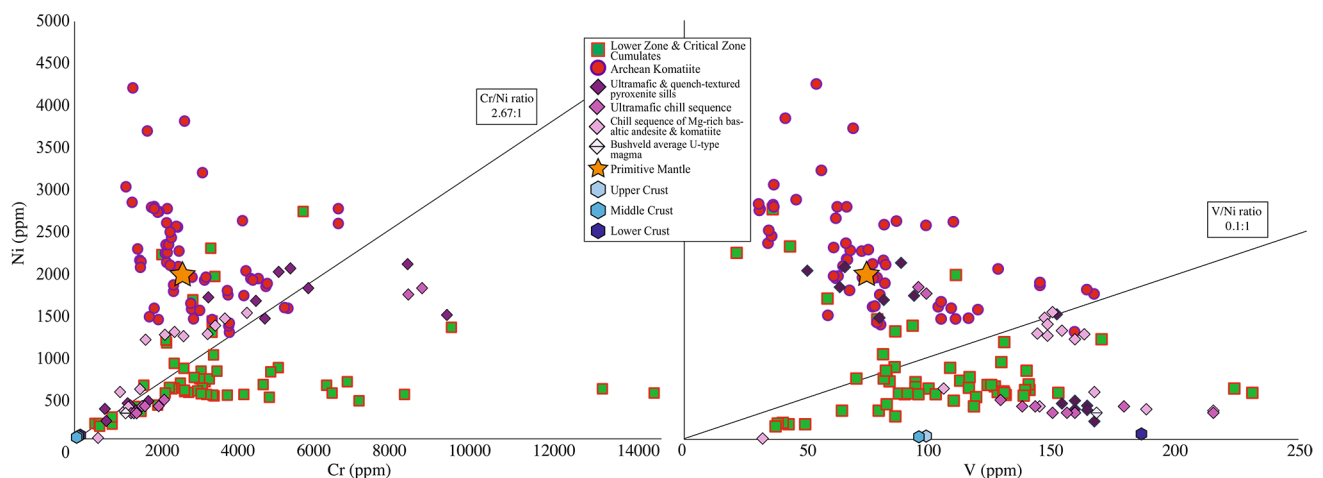


**Fig. 1** Trace-element compositions of Rustenburg Layered Suite (RLS) Lower- and Critical Zone silicate cumulate rocks (green squares; Maier et al. 2013); average Kaapvaal craton Archaean komatiite (red circles; Robin-Popieul et al. 2012; spinifex analyses removed); upper, middle, and lower continental crust (light to dark blue hexagons; Gao et al. 1998); primitive mantle (orange stars; Lyubetskaya and Korenaga 2007); and proposed quenched primitive RLS magmas (diamonds; Sharpe and Hulbert 1985, dark purple; Barnes 1989, light pink; Wilson 2012, dark pink, spinifex analysis removed; Maier et al. 2016, light purple). The ratios of Cr/Ni and V/Ni in the RLS mafic-ultramafic Lower- and Critical Zones are notably higher than primitive mantle values, and greatly in excess of the Cr/Ni and V/Ni ratios

in well characterised Archaean komatiites. They are also higher than minor rock types in the RLS interpreted to possibly represent relatively unhybridised komatiitic parental magmas. Where overlap of these rocks with the Lower- and Critical Zone cumulates do occur, they are either relatively low in Cr and Ni for typical komatiites, or contain considerably more Ni relative to Cr than the cumulates. If hybridised komatiite magmas were responsible for the formation of the RLS and its chromitites, much higher Ni values would be expected for average Lower- and Critical Zone silicate cumulate rocks, particularly considering the fraction of olivine in some of the cumulates and the fact that pyroxene:melt partitioning coefficients for Ni, Cr, and V are considered to overlap for basaltic magmas (e.g. Bédard 2007)

in a relevant area of pressure-temperature (P-T) space, in constant-composition systems without magma extraction. This allowed the peritectic crystals that increase in abundance with melt to be identified. Second, we investigated sequential magma extraction events that may occur, and the magma compositions produced along two different approximately adiabatic melting paths. Magma extraction was set to occur when melt volume exceeded 5 wt% – within the threshold suggested by Winter (2010) – with peritectic crystal entrainment set to occur when these crystals were produced with the melt. Only the peritectic crystals produced in the preceding step along the P-T path were entrained into the extracted magma, thus representing a minimum estimate of entrained peritectic material. If no peritectic phases were produced, only melt was extracted. Lastly, we modelled magma ascent and fractional crystallisation of selected magma batches emplaced as sills into the crystal mush at the base of a hypothetical 0.3 GPa upper-crustal magma chamber, over the cooling interval down to ~ 1000 ºC. Solids in the magma at emplacement were modelled as undergoing immediate density separation on intrusion.

## Modelling details

Thermodynamically constrained petrological calculations were performed using the Rcrust software (Mayne et al. 2016), which emulates open-system behaviour via a path-dependent calculation strategy that allows bulk compositional change via processes of mass transfer. Rcrust version 2020-04-19 was used with the Holland and Powell (2011) thermodynamic dataset and the 2020 revised hp633ver. dat thermodynamic data file from Perple_X in the NKCF-MASTCr (Na$_2$O-K$_2$O-CaO-FeO-MgO-Al$_2$O$_3$-SiO$_2$-TiO$_2$-Cr$_2$O$_3$) chemical system. MnO was excluded from the modelling due to the absence of MnO as a component in the igneous melt model. The following phase solution (activity-composition) models were used: Cpx(HGP) for clinopyroxene, Gt(HGP) for garnet, O(HGP) for olivine, Opx(HGP) for orthopyroxene, Sp(HGP) for spinel, and melt(HGP) for melt (Holland et al. 2018); Fsp(C1) for plagioclase and potassium-feldspar (Holland and Powell 2003); and Ilm(WPH) for ilmenite (White et al. 2000). The modelling method applied has been demonstrated to produce a high level of consistency between the modelling and experimental results on peridotite partial melting under upper-mantle

conditions (Otto et al. 2023). Adjustments made to solution model parameters are listed in the Supplementary Material.

## Identifying peritectic phases in the modelling

To identify areas of peritectic crystal production with high probability of crystal entrainment to the magma, for each of the peridotitic compositions investigated (Table 1), P-T phase diagrams and phase abundance maps were modelled between 1300 ºC and 1600 ºC and 3.0 to 1.5 GPa. P-T areas characterised by an increase in the abundance of a crystalline phase as a function of partial melting were identified as areas of peritectic phase production. It is important to note that such considerations are made in terms of the increase or decrease in abundance of the mineral phase/s as a consequence of the melting reaction, i.e., along decompression paths, phase changes due to pressure-induced mineral stability transitions (e.g., garnet to spinel) are not considered peritectic.

A volatile-free system was modelled because the peridotite solidus is lowered by both H$_2$O and CO$_2$. A consequence of this is that our modelling maps out behaviour in the highest possible temperature range. Introduction of volatiles would lower the solidus temperature and increase the peritectic crystal yield.

## Quantifying peritectic phase production and modelling magma extraction

To investigate magma extraction, with the possibility of peritectic phase entrainment, we investigated partial melting and magma extraction for rocks undergoing approximately adiabatic decompression. Lower- and higher-temperature decompression paths were investigated. Where peritectic phase production was identified, the amounts of peritectic phases were quantified by calculating the increase in their abundance for each P-T step along the path.

## Adiabatic ascent paths

To simulate adiabatic decompression, modelling was performed using the 502 peridotite composition (Table 1) across 4.5 to 1.5 GPa – thus ensuring that the starting P-T conditions were located below the solidus – with a 0.02 GPa pressure resolution. To accommodate the heat of

**Table 1** Compositions of the peridotitic sources used for Rcrust petrological modelling

|  | SiO$_2$ | TiO$_2$ | Al$_2$O$_3$ | Cr$_2$O$_3$ | FeO$_{tot}$ | MgO | CaO | Na$_2$O | K$_2$O | Sum |
|---|---|---|---|---|---|---|---|---|---|---|
| 502[1] | 44.69 | 0.32 | 4.04 | 0.39 | 9.0 | 37.93 | 3.21 | 0.22 | 0.19 | 100.00 |
| KLB-1[2] | 44.65 | 0.16 | 3.60 | 0.31 | 8.13 | 39.37 | 3.45 | 0.30 | 0.02 | 100.00 |
| MM3[3] | 45.67 | 0.11 | 3.99 | 0.68 | 7.21 | 38.44 | 3.58 | 0.31 | 0.00 | 100.00 |
| HK66[4] | 48.35 | 0.22 | 4.91 | 0.25 | 9.97 | 32.57 | 2.99 | 0.66 | 0.07 | 100.00 |

[1]Danchin 1979; [2]Takahashi 1986; [3]Baker and Stolper 1994; [4]Hirose and Kushiro 1993

melting and subsequent departure of the temperature path from the geotherm, the P-T path trajectories above the solidus were modelled to follow a decreasing temperature path that displayed the steadiest values of entropy of the bulk system during decompression. This yielded approximately adiabatic paths with potential temperatures (McKenzie and Bickle 1988) of 1260 ºC and 1450 ºC for paths 1 and 2, respectively. For the three other compositions studied, the adiabatic paths utilised mimic that of the paths applied in the modelling of the 502 source; note that, in reality, they would all vary by a small amount.

During magma extraction events, entropy loss was noted, but was minimal, and the values subsequently return to the entropy of the magma prior to extraction (see the Supplementary Material).

## Magma extraction events

Melt formation, and entrainment of peritectic phases into the melt on segregation from the source, will create magmas with chemical compositions that reflect a combination of the mass of segregated melt and the compositions and abundances of the entrained crystals. Sequential magma extraction events were performed along the described adiabatic paths using the 502 peridotite composition. Extraction was set to be triggered whenever melt exceeded 5 wt% in the source. To approximate a degree of melt retention on grain boundaries, an amount of 10% of the original melt was left unextracted. Peritectic phase entrainment was modelled by considering a scenario in which only the peritectic crystals produced in the preceding step along the P-T path were entrained, with peritectic crystals produced in previous steps assumed to have recrystallised into structures too large for entrainment. As the temperature steps used in this modelling were small ($\sim 0.5$ ºC), this represents a minimum estimate of the amount of peritectic material that may be entrained. Note that, due to reaction between the entrained peritectic crystals and the melt on adiabatic ascent, melt proportions grow relative to the crystal fraction and the crystal assemblages and compositions continually change to maintain equilibrium.

## Entrainment modelling of peritectic phases

Quantification of the proportion of peritectic phases produced, if any, was calculated using the Rcrust 'Delta' function. Since peritectic phases are produced as products of incongruent melting reactions, they must increase in abundance during melting. The Delta function allows the user to specify only the portion of a predicted phase that increases in abundance during melting to be quantified and included in extraction simulations. In other words, for a predicted

phase, the Delta function calculates the incremental difference between the point of extraction (point *b*) and a specified previous point (point *a*), such that the change in the phase proportion from point *a* to point *b* can be incorporated in the extraction simulation. The Delta function can be expressed as:

$$delta\{phase; x\_a; y\_a; unit\} \tag{1}$$

where *phase* is the phase intended for extraction, $x\_a$ and $y\_b$ describe the location of point *a*, and *unit* can be measured in mol%, vol%, or wt%. Point *a* can specified in two ways: (i) 'prev_ext_X', where X can be any phase of choice from which the delta change must be calculated, or (ii) 'prev_ext', where the name of the extracting phase is the default choice for the delta calculation.

In our modelling, an estimate on the behaviour of peritectic entrainment was modelled using the 'prev_ext' specification discussed above, where the delta change in wt% of the peritectic phases to be entrained are calculated from the point of extraction to one P-T point (which is dependent on the adiabat) before the extraction.

## Fractional crystallisation

The sequential magma extraction simulations described above resulted in a number of extraction events, each producing a model melt or magma. To simulate intrusion and fractional crystallisation in an upper-crustal sill or magma chamber, magma emplacement was modelled to follow isobaric cooling paths at 0.3 GPa, starting at a temperature determined by the relevant ascent path of selected model magmas.

The crystallisation of emplaced magma batches was modelled assuming immediate density separation of the phases at each cooling step. To simulate this segregation of the crystals, the 'any_phase' expression in Rcrust was used and allows generic arguments for all phases that may be predicted to be set, given that the phase does not have a phase extraction proportion already specified. Subsequently, for each P-T point along the cooling path, the melt phase extraction proportion was specified as 0%, and for all other predicted phases (any_phase), the extraction proportion was set to 100%. This results in a scenario in which the continued crystallisation of the evolving magma can be simulated, with already crystallised phases 'leaving' the magma system as they settle onto the chamber floor, immediately excluding these phases from contributing to the reactive bulk composition in future steps. The abundance and density (amongst numerous other calculated parameters) of the crystallising phases for each P-T step can thus be gathered and quantified in a thermodynamically evolving system, allowing

predictions of the possible cumulates that could form as a result of gravity settling.

## Results

The resulting pseudosections and phase abundance maps produced from the first step of the modelling are displayed in Fig. 2, allowing the partial melting behaviour of four representative peridotites (Table 1) to be investigated. The volatile-free solidi range from 1300 ºC at ~ 1.3–1.7 GPa to ~ 1470–1550 ºC at 3.0 GPa, as shown by the pseudosections in Fig. 2a-d. Analysis of the phase abundance maps (Fig. 2e-h) show, in the P-T region of interest, the existence of subdomains where spinel and orthopyroxene were identified as peritectic products of partial melting that increased in abundance as melting progressed. For much of the super-solidus space, for all four compositions, the only peritectic phase to form is orthopyroxene, which is produced within a wedge-shaped band that narrows with increasing pressure. Peritectic spinel is present at low pressure for three of the four peridotites studied and is superimposed on the orthopyroxene fields in Fig. 2. Detailed annotations for the interpretation of the phase abundance maps and the melting reactions are indicated for the 502 peridotite in Fig. 2e, as the 502 composition was utilised throughout all modelling routines: With increasing degrees of melting, both orthopyroxene and spinel (where applicable) become reactants in the partial melting reactions. In the case of orthopyroxene, this transition from peritectic product to reactant in the incongruent melting reaction is triggered by the disappearance of clinopyroxene. In the case of peritectic spinel, the trigger is the disappearance of garnet.

By utilising the pseudosections and phase abundance maps, plots of phase abundances along a nearly adiabatic decompression path (which is indicated on Fig. 2a & e) can be produced and are displayed for each of the four peridotites in Fig. 3. The production of peritectic orthopyroxene in a constant-composition scenario (no magma extraction) due to reactions that consume garnet and clinopyroxene, is observed for all compositions investigated. Figure 4 displays the abundance of $Cr_2O_3$ in all of the relevant phases along the same path as in Fig. 3, for each peridotite. These plots indicate that the $Cr_2O_3$ content of garnet increases as garnet mode decreases, and once garnet is consumed, the most $Cr_2O_3$-rich phase is peritectic orthopyroxene.

Having identified peritectic orthopyroxene production during partial melting as a result of decompression in a constant-composition scenario, the results from the modelling of sequential magma extraction along the two adiabatic paths using the 502 peridotite source is summarised in Fig. 5; the extraction conditions and weight fractions of

melt and entrained peritectic phases are displayed. Note that the melt production along the cold path was sufficient only to trigger one extraction event. Two extractions are crystal-free (magmas B2 and B6), and despite generally low peritectic crystal to melt ratios, extraction event B4 produces a crystal-rich magma with > 40% entrained peritectic orthopyroxene.

The results from the simulation of the emplacement of selected magma batches from the extraction modelling (Fig. 5) into an upper-crustal magma chamber, and subsequent crystallisation, is shown in Fig. 6, which displays the resulting variation in phase abundances as a function of decreasing temperature, and the igneous stratigraphy that would be produced by selected magma batches, if intruded as sills. The amounts of melt remaining in the sill at the end of the cooling temperature interval are also displayed. From Fig. 6, the crystallisation behaviour of magma B2, which involves no peritectic phase entrainment (b), shows less cumulate formation along the cooling path, and no chromite (b(i)). As displayed in (c) and (d), magmas with entrained peritectic orthopyroxene (magmas B4 and B5, respectively) intrude as chromite- and olivine-bearing slurries (c(i)) or show chromite crystallising at lower temperature (d(i)). Crystallisation due to cooling of the B4 magma in the sill results in the formation of a chromitite layer, followed by pyroxenite and then norite, or, as illustrated, if plagioclase segregates by density, an anorthosite layer will result following loss of the residual melt. Note that the removal of orthopyroxene on the ascent path is important to chromite formation. As a result of the lower intrusion temperature of magma A1 (a), the magma is predicted to intrude the crustal chamber as an olivine-bearing slurry. The magma is $Cr_2O_3$-bearing, but this Cr is contained in orthopyroxene and therefore cannot undergo density segregation from the silicate minerals, thus resulting in no chromite formation.

Using the phase abundance and density data collected during crystallisation modelling routines, the plot in Fig. 7 shows the variation in density for the different crystallising phases during cooling in a magma chamber in the upper crust. This data was utilised to produce the igneous stratigraphy (example cumulates) plotted in Fig. 6. Note that ferromagnesian silicate and oxide minerals that crystallised together, as a function of cooling in a sill, were not modelled as undergoing density segregation from another, but were regarded as separating from the near-neutral-buoyancy plagioclase by this mechanism. Melt remaining at the end of the crystallisation sequence was modelled as draining off by filter pressing due to compaction (Connolly and Schmidt 2022) from layers deposited by overlying sills, or other deformation processes.
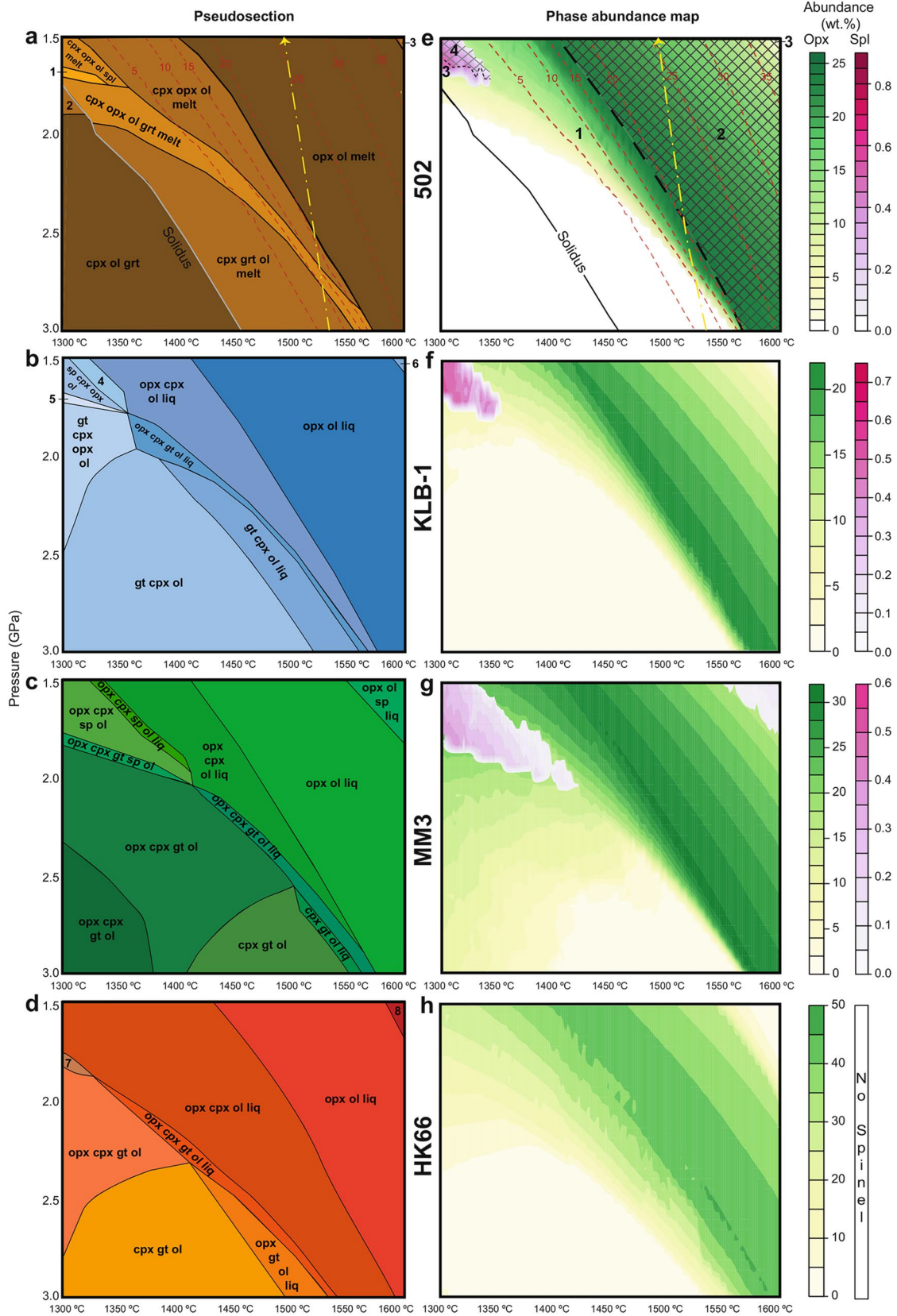
Pseudosection / Phase abundance map

**Fig. 2** The results of petrological modelling to investigate and identify peritectic phase formation during partial melting of representative mantle peridotite sources in the upper subcratonic mantle. **a-d** Constant-composition P-T sections (pseudosections) for four different peridotite compositions that feature prominently in the literature (**a** – 502; **b** – KLB-1; **c** – MM3; **d** – HK66), within the P-T range of 1300 to 1600 ºC and 1.5 to 3.0 GPa. **1**: Cpx Grt Opx Ol Spl Melt; **2**: Cpx Grt Opx Ol; **3**: Opx Ol Spl Melt; **4**: Cpx Opx Ol Spl Melt; **5**: Cpx Grt Opx Ol Spl; **6**: Ol Melt; **7**: Cpx Opx Ol; **8**: Ol Melt. **e-h** The abundance of orthopyroxene (green) and spinel (pink) for each of the compositions, where applicable. Analysis of phase abundance changes are described here for the 502 peridotite source (**e**) and is generally applicable to the other sources. The yellow to green field (1) to the left of the heavy black dashed line represents the area of peritectic orthopyroxene production, where orthopyroxene abundance increases with melt volume (in wt%, displayed as red, short-dash contour lines). In this area, orthopyroxene abundance increases from 0 to >25 wt% (colour change from white to dark green). The cross-hatched, green to yellow field (2) to the right of the black dashed line indicates the area where orthopyroxene is consumed by melting, as is evident by the orthopyroxene abundance change from 25 to <10 wt% (colour change from dark green to yellow). Two small areas of P-T space (3), superimposed on the orthopyroxene fields, indicate peritectic spinel formation, followed by its consumption (4; cross-hatched) at higher temperature and/or lower pressure. Thus, the production of peritectic crystals, the nature of these crystals, and their abundance, is strongly controlled by pressure, temperature, and the degree of melting. Within the modelled area there are two broad regions where melting of the 502 peridotite produces no new mineral phases and the proportion of all crystal phases in the source decreases as a function of increasing melt volume. The first is the white area above the solidus, and the second is area 2. These areas hold no potential for the entrainment of peritectic crystals. Cpx: clinopyroxene; Grt: garnet; Ol: olivine; Opx: orthopyroxene; Spl: spinel

## Discussion

### The double-peritectic model for silicate & chromite layering

Our results show that during partial melting of a garnet peridotite in the upper mantle, peritectic orthopyroxene is produced over a wedge-shaped P-T domain that is closer to the solidus at low pressure and separates from the solidus and narrows at higher pressure (Fig. 2). Orthopyroxene has a crystal-chemical affinity for Cr (Jean and Shervais 2017; Fig. 4) and the entrainment of peritectic orthopyroxene fundamentally changes the magma chemistry to be enriched in Cr. This has profound consequences for the assemblage of crystals in the magma (Fig. 5) and crystallisation behaviour (Fig. 6). Our modelling demonstrates that, during magma ascent, melt volume grows by the incongruent melting of the orthopyroxene cargo (Fig. 8), producing new peritectic chromite and olivine.

The formation of peritectic chromite depends on both the amount of orthopyroxene entrained to the magma, and the amount of orthopyroxene that undergoes incongruent melting on magma ascent, which is a function of temperature and amount of decompression (Fig. 8b). Magmas leaving

their sources as melt only (extraction B2, Fig. 6b) cannot form chromite crystals as the Cr dissolved in melt (0.16 wt%; see the Supplementary Material) is easily accommodated in pyroxene which crystalises prior to chromite saturation. Similarly, magmas entraining peritectic crystals that originate at relatively low pressure and temperature (extraction A1; 0.23 wt% $Cr_2O_3$) do not melt enough pyroxene on ascent to produce peritectic chromite. In contrast, extracted magmas bearing peritectic orthopyroxene that originate at high temperature, produce peritectic chromite crystals on ascent (extraction B4; $Cr_2O_3$ in the magma is increased from 0.26 wt% to 0.81 wt% due to the presence of peritectic orthopyroxene), or crystalise chromite during cooling after emplacement (extraction B5; 0.26 wt% to 0.47 wt% $Cr_2O_3$ increase). Chromitite layers will most readily be produced by magma batches such as B4, where the magma injects as an olivine- and chromite-bearing slurry, with the density contrast between these phases ensuring efficient separation, at least on scale of meters, forming a chromitite layer at the base of the sill (Fig. 6c). Further cooling can produce layers of dunite, pyroxenite, norite, and possibly anorthosite, whereas inefficient crystal separation can produce layers of dunite, gabbro, and norite, with interstitial chromite. Should magma drainage occur shortly after intrusion of the sill, potentially only a chromitite or a chromitite plus a dunite layer would result (Fig. 6c(i)).

Peritectic crystal entrainment depends on peritectic crystals nucleating as independent crystals in the melt, as well as channelised, sufficiently rapid melt flow to remove these crystals from the source and incorporate them into the magma. Experiments using glass starting materials have confirmed peritectic orthopyroxene formation during mantle melting (e.g., Grove et al. 2013; Kinzler 1997). In the case of the mantle peridotites we have studied, peritectic orthopyroxene would be the most common and abundant phase produced with melt in the subcratonic upper mantle, and the first orthopyroxene phase to appear (Figs. 3 and 4). Experiments on crustal compositions using mineral mixtures (Stevens et al. 1997), where the kinetics of mineral dissolution, intra-crystalline diffusion and nucleation control the distribution of phases, commonly show that peritectic orthopyroxene nucleates easily and abundantly (Zellmer et al. 2016) in melt pools (Zhang et al. 2010). Thus, with no prior orthopyroxene on which to nucleate, the peritectic orthopyroxene is likely to form as small, discrete crystals suspended in the melts (Erdmann et al. 2012).

There is continuous debate about how rapidly melt can be extracted from mantle source rocks (Rees Jones and Rudge 2020). Some studies of melt production and extraction from the mantle regard both as slow processes (e.g., Bulau et al. 1979; McKenzie 1984). However, as in the crust, mantle melting occurs in different tectonic settings and, in some

**Fig. 3** Phase abundances along an approximately adiabatic decompression path from below the solidus to 1.5 GPa, showing peritectic orthopyroxene production in a constant-composition scenario (no magma extraction) for four different peridotite compositions that feature prominently in the literature (Table 1). The adiabatic path followed is illustrated in yellow dash-dot on the P-T and phase abundance diagrams of the 502 composition (Fig. 2a & e), The paths followed for the three other compositions approximate this path (see Methodology). The formation of melt and peritectic orthopyroxene by reactions that consume garnet and clinopyroxene are observed in all four compositions
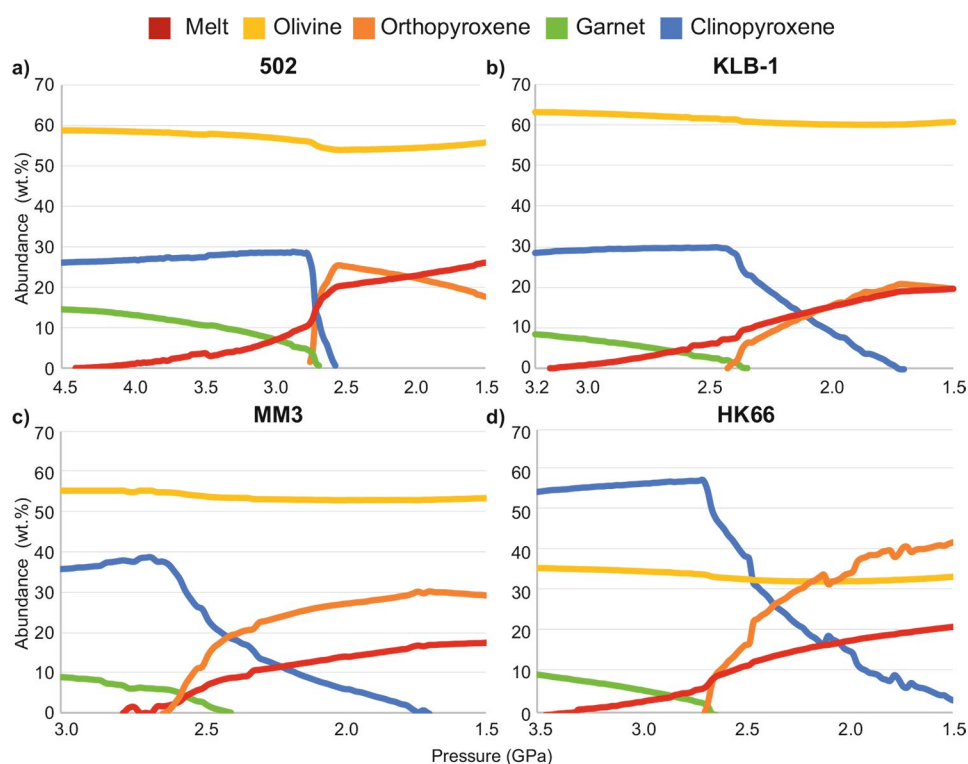


situations, the rates of P-T change or activities of volatile components are likely sufficient to allow rapid melting and melt extraction. This is supported by several lines of evidence. For many alkali-rich mafic magmas, flow through the mantle must be channelised and fast, as such compositions are strongly out of equilibrium with typical mantle rocks (Keleman et al. 1997). Additionally, information on rates of basalt accumulation and on the required minimum rates of ascent of a variety of magma types that exhume mantle xenoliths demonstrate clearly that mantle melts are produced, segregate and ascend rapidly enough to transport even decimetre-sized mantle xenoliths and peritectic products from deep staging chambers to the surface (Li et al. 2012; O'Reilly and Griffin 2010; Sun et al. 2018). As such, it is rather apparent that an accelerated, chemically isolated mechanism of melt production and transport is unavoidable (Keleman et al. 1997; Spiegelman and Kenyon 1992).

Melt extraction from partially molten mantle regions has been widely attributed to the formation of high-permeability pathways through reactive-infiltration instability (e.g., Chadam et al. 1986; Daines and Kohlstedt 1994), defined as the positive feedback between melt flow and reaction. Sandwich experiments of partially molten rock between a porous sink and a melt source (Pec et al. 2017) indicated that melt fractions as low as 0.04 show the development of channels in the partially molten rock, with increased melting (greater than 0.2) forming multiple channels, and considerable melt pooling at melt fractions at or greater than 0.05 (Miller et al.

2014). Importantly, peritectic olivine phenocrysts of various sizes that were initially randomly distributed in the melt source, collect in large numbers during infiltration (Pec et al. 2017). This requires the olivine crystals to be advected toward major channel entrances by focused melt flow, where crystals become locally entrained in the melt-rich channels forming due to pyroxene consumption. In Fig. 3, olivine is the slowest consumed reactant, suggesting a similar reaction-induced channelisation mechanism is likely, given that the permeability is increased by the reaction. Since intracratonic plume and rift settings are characterised by high rates of mantle melting (Van Wijk et al. 2001; White 1993) and evidence for short magma transport times is well-established (Connolly et al. 2009; O'Reilly and Griffin 2010; Rees Jones and Rudge 2020), the likelihood of strong melt channelling and rapid magma extraction will favour peritectic phase entrainment into the magma in the source if it is produced by the melting reaction, without its presence having a significant effect on magma viscosity (Costa et al. 2009).

There are two important aspects in the findings of this study. Considering that the crystallisation of the RLS occurred within $1.02 \pm 0.63$ Ma and required large magma volumes ($> 5$ km$^3$/year) with rapid accretion over $< 100$ ka (Zeh et al. 2015), the likelihood of rapid melting, magma extraction and magma ascent suggests the entrainment of peritectic orthopyroxene. Second, hotter magmas that formed at higher pressure will undergo more decompression, and this
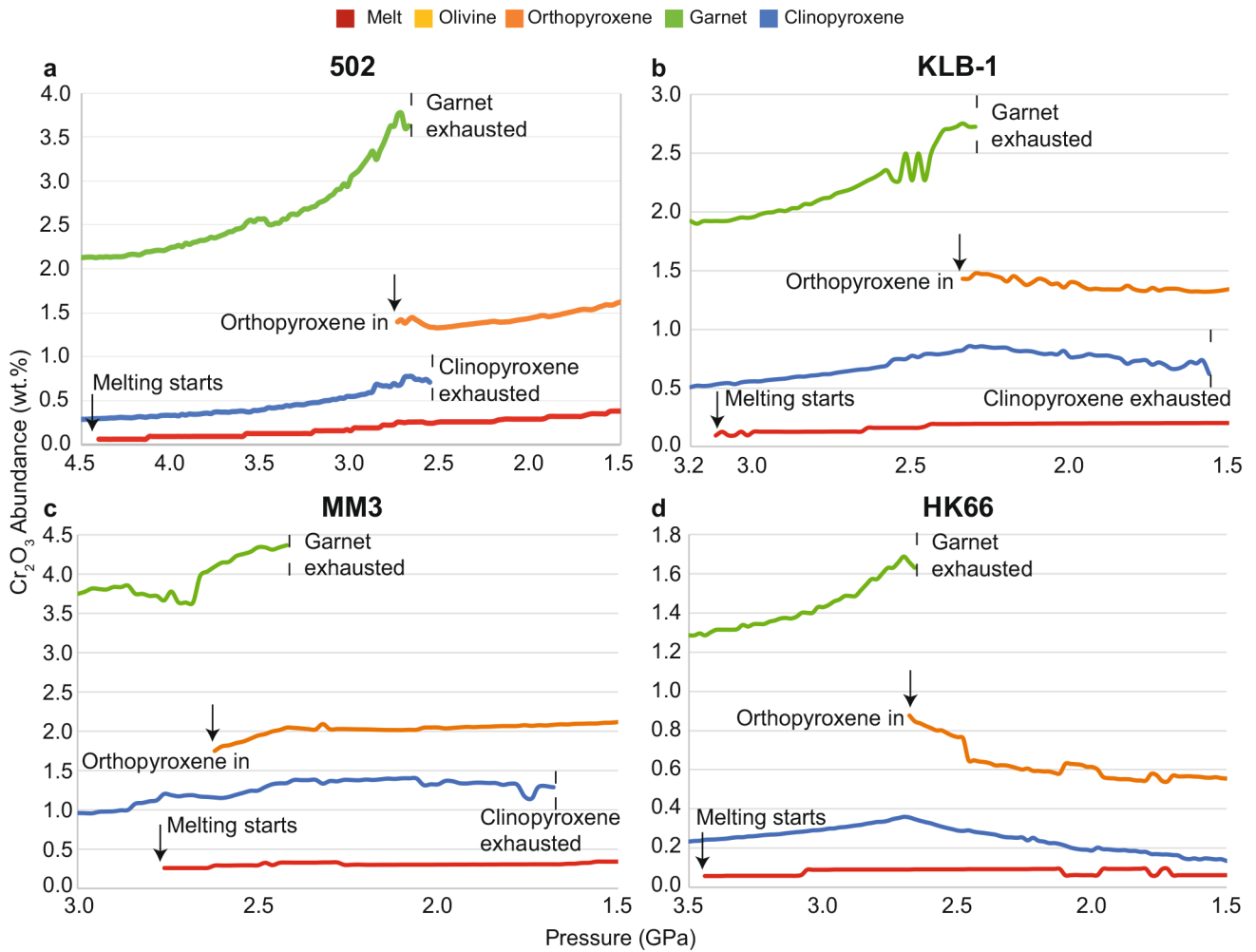
**Fig. 4** The abundance of the $Cr_2O_3$ in the relevant Cr-bearing phases along the modelled decompression path (illustrated in yellow dash-dot on the P-T diagram of the 502 composition (Fig. 2a)) for the peridotite compositions studied. Note that, for all the peridotite sources, as the garnet mode decreases, the $Cr_2O_3$ content of garnet increases and on garnet disappearance, peritectic orthopyroxene becomes the most $Cr_2O_3$-rich phase. When considering the $Cr_2O_3$ abundance in the relevant phases in relation to partitioning data from Davis et al. (2013), the partitioning coefficient for Cr between melt and orthopyroxene are well within the range reported (see the Supplementary Material)



**Fig. 5** The results of thermodynamic modelling of the melting reactions and magma extraction events in a representative garnet peridotite (502, Table 1) during decompression. **a** Plot displaying the P-T conditions of the magma extraction events along the two approximately adiabatic ascent paths. **b** The components of the magma batches on extraction from the source, discussed in-text
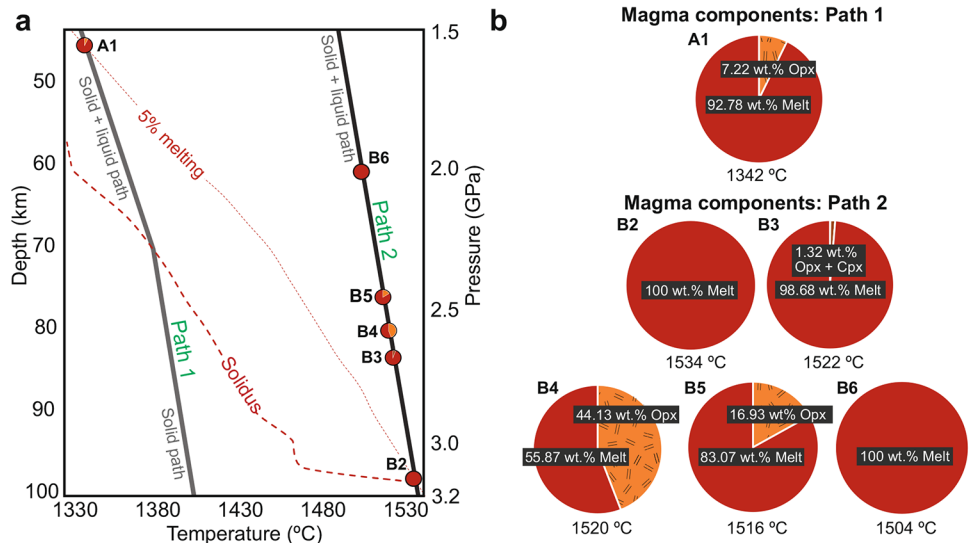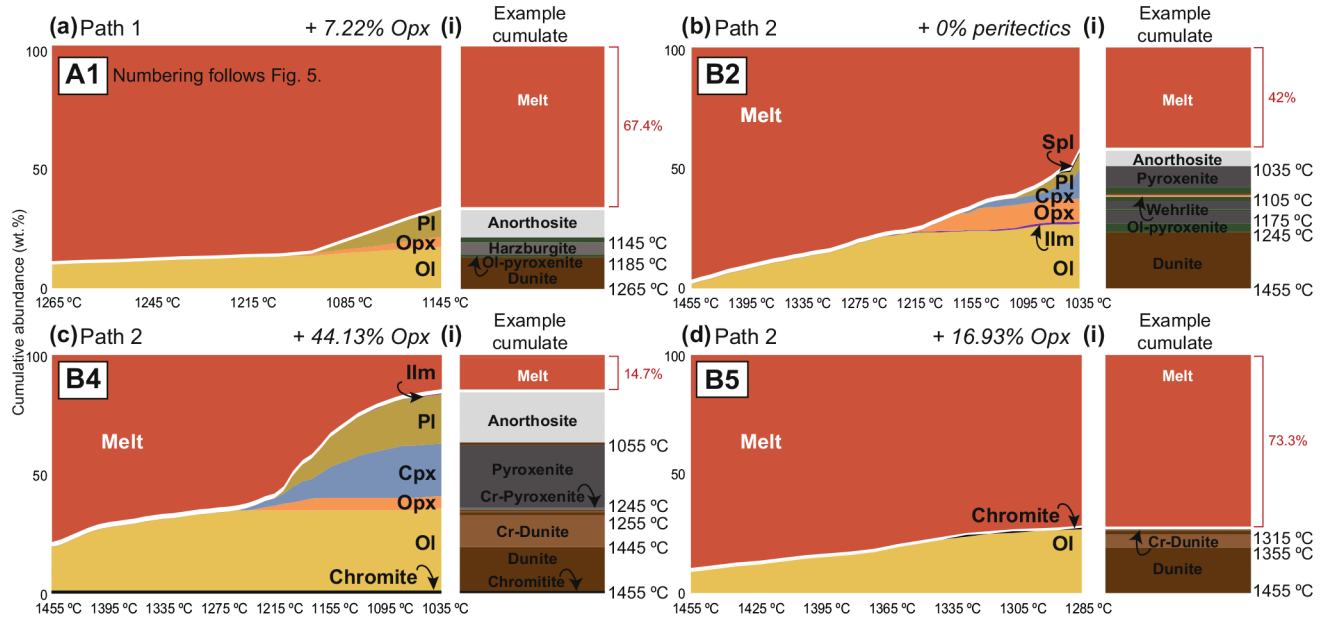
**Fig. 6** The results of thermodynamic modelling from the emplacement of the resulting model magmas at 0.3 GPa, displayed as plots of cumulative phase abundance, and the igneous stratigraphy predicted for cooling from emplacement temperature, assuming that the crystals present at emplacement undergo perfect density-driven segregation (as outlined in Fig. 7). The plots are labelled according to the extraction event in Fig. 5 that produced the model magma. The cumulative phase abundance displayed at each point along the temperature interval reflects the sum of all of the phases produced during the crystallisation sequence up until that point. Note that the stratigraphy is illustrative of that which would be produced by significant cooling in the sill. If the magma drained out of the structure following settling of the chromite from the slurry, a chromitite layer would be the only marker of intrusion. If the magma did not inject as a sill but mixed with resident magma in a chamber, then a Cr-enriched and chromite saturated magma may result. Ilm: ilmenite; Pl: plagioclase
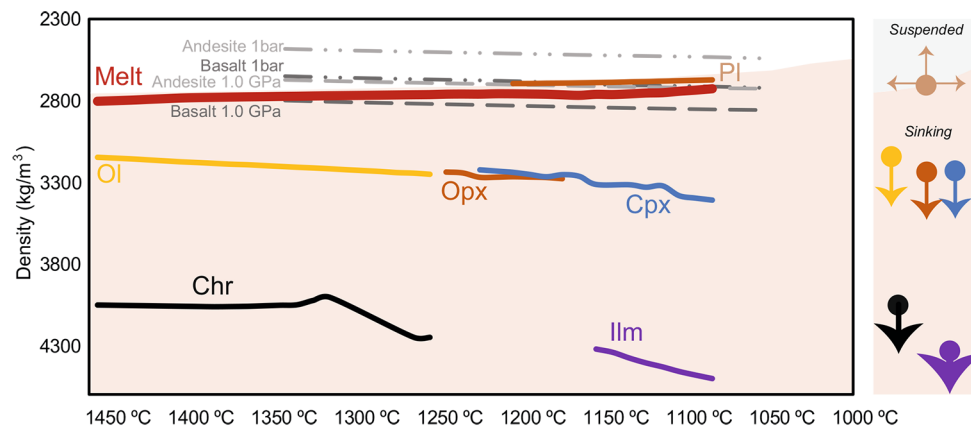


**Fig. 7** A plot of the modelled phases in the magma during fractional crystallisation and the thermodynamically calculated density values as a function of temperature along the 0.3 GPa isobaric crystallisation path for extraction event B4 (solid lines), as numbered in Fig. 5a-b. Density estimates for typical basaltic (dark grey dashed) and andesitic magmas (light grey dashed) at 1 bar and 1.0 GPa (Lesher and Spera 2015) are displayed as references for comparison with the modelled melt density values. Vectors on the right indicate the calculated effects of the density differences between the crystalline phases and the melt. Chr: chromite

results in a greater yield of chromite in the sill. As such, the chromitite layers of the RLS would represent magma production events that favoured both peritectic orthopyroxene entrainment and derivation from sufficient depth to produce hot, chromite-crystal laden magmas that were delivered into the sill or a crustal chamber, or that produced chromite during cooling. In this way, some of the proposed processes

for the formation of RLS chromitites, such as the growth of chromite crystals on a cold lower contact surface (Latypov et al. 2018) or gravity-driven fractional crystallisation (e.g., Naldrett et al. 2012), may be equally applicable to our proposed sills, but these would represent second-order processes. The double-peritectic model thus provides a simple, first-order, chemically and thermodynamically constrained
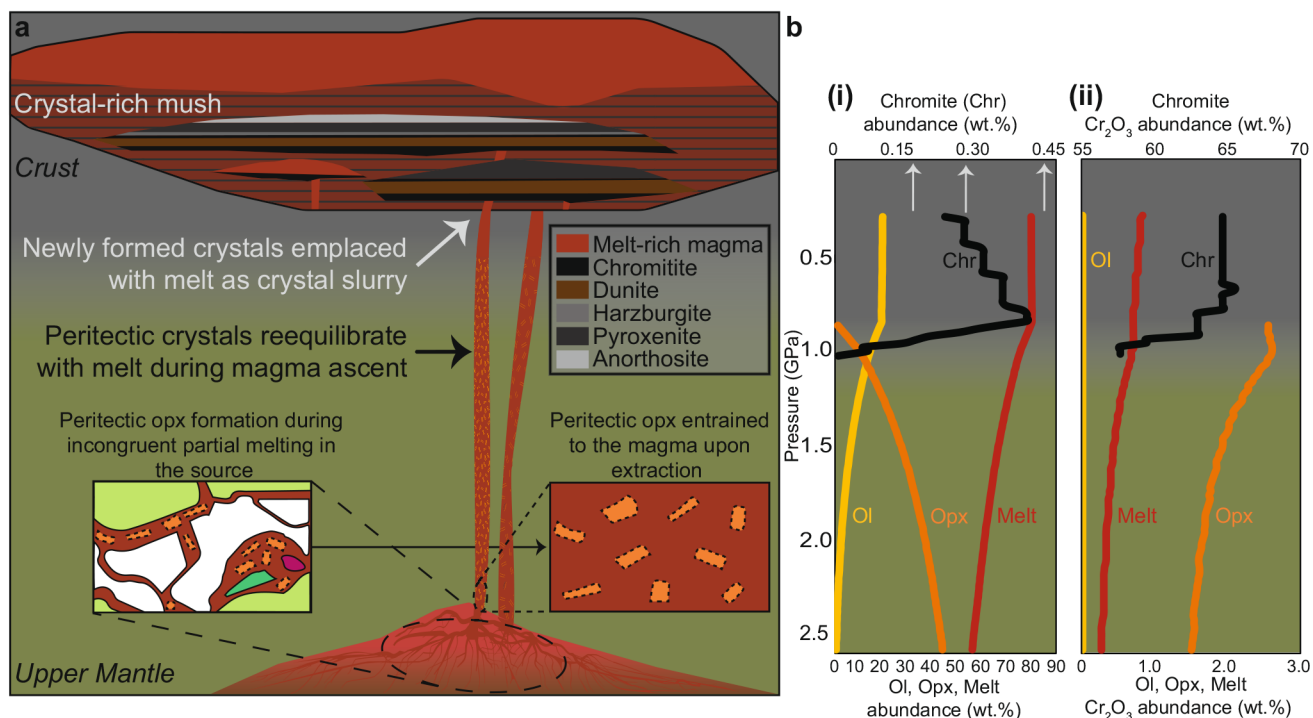
**Fig. 8** A physical model for the generation of chromitite and silicate layering through entrainment of peritectic crystals in the upper mantle source during magma extraction. **a** Under specific mantle conditions, incongruent partial melting reactions produce new peritectic crystals at the melting sites. A proportion of these crystals may be entrained to the melt on segregation from the source. Changing P-T conditions during approximately adiabatic ascent consume the entrained peritectic crystals, and recrystallisation at mid- to shallow crustal conditions produces a melt-dominated magma with new crystal phases in suspension. Emplacement of sills within or below magma chambers of this crystal-mush can produce layering similar to that found in the lower portions of the RLS, assuming effective density separation of crystals in the magma chamber as the magma cools. The upward migration of the remaining melt is achieved by filter pressing due to compaction, or due to the decreasing density of melt as the crystalline phases settle out. **b** (i) The consumption of the entrained peritectic orthopyroxene during ascent is displayed by its decrease in abundance as magma travels along the adiabat. The reaction of this Cr-rich, ferromagnesian phase with the melt results in the crystallisation of peritectic olivine and ultimately, the formation of peritectic chromite at low pressure. (ii) As the amount of orthopyroxene decreases due to the melting reaction, its $Cr_2O_3$ content increases until saturation. At this point, Cr-spinel appears, and becomes more $Cr_2O_3$-rich as decompression continues

process in which the entrainment of peritectic orthopyroxene in the source and its digestion by the ascending magma can explain the formation of the RLS chromitites.

## Declarations

# References

Baker MB, Stolper EM (1994) Determining the composition of high-pressure mantle melts using diamond aggregates. Geochim Cosmochim Acta 58:2811–2827. https://doi.org/10.1016/0016-7037(94)90116-3

Barnes SJ (1989) Are Bushveld U-type parent magmas boninites or contaminated komatiites? Contrib Miner Petrol 101:447457. https://doi.org/10.1007/BF00372218

Bédard JH (2007) Trace element partitioning coefficients between silicate melts and orthopyroxene: parameterizations of D variations. Chem Geol 244:263–303. https://doi.org/10.1016/j.chemgeo.2007.06.019

Bulau JR, Waff HS, Tyburczy JA (1979) Mechanical and thermodynamic constraints on fluid distribution in partial melts. J Phys Res 84:6102–6108. https://doi.org/10.1029/JB084iB11p06102

Chadam J, Hoff D, Merino E, Ortoleva P, Sen A (1986) Reactive infiltration instabilities. IMA J Appl Math 36:207–221. https://doi.org/10.1093/imamat/36.3.207

Connolly JAD, Schmidt MW (2022) Viscosity of Crystal-Mushes and implications for Compaction-Driven Fluid Flow. J Phys Res 127: e2022JB024743. https://doi.org/10.1029/2022JB024743

Connolly JAD, Schmidt MW, Solferino G, Bagdassarov N (2009) Permeability of asthenospheric mantle and melt extraction rates at mid-ocean ridges. Nature 462:209–212. https://doi.org/10.1038/nature08517

Costa A, Caricchi L, Bagdassarov N (2009) A model for the rheology of particle-bearing suspensions and partially molten rocks. Geochem Geophys Geosyst 10. https://doi.org/10.1029/2008GC002138

Daines MJ, Kohlstedt DL (1994) The transition from porous to channelized flow due to melt/rock reaction during melt migration. Geophys Res Lett 21:145–148. https://doi.org/10.1029/93GL03052

Danchin RV (1979) Mineral and Bulk Chemistry of Garnet Lherzolite and Garnet Harzburgite Xenoliths from the Premier Mine, South Africa. American Geophysical Union, Washington. https://doi.org/10.1029/SP016p0104

Davis FA, Humayun M, Hirschmann MM, Cooper RS (2013) Experimentally determined mineral/melt partitioning of first-row transition elements (FRTE) during partial melting of peridotite at 3 GPa. Geochim Cosmochim Acta 104:232–260. https://doi.org/10.1016/j.gca.2012.11.009

Eales HV (2000) Implications of the chromium budget of the western limb of the Bushveld Complex. S Afr J Geol 103:141–150. https://doi.org/10.2113/103.2.141

Eales HV, Costin G (2012) Crustally contaminated komatiite: primary source of the chromitites and marginal, lower, and critical zone magmas in a staging chamber beneath the Bushveld Complex. Econ Geol 107:645–665. https://doi.org/10.2113/econgeo.107.4.645

Erdmann S, Scaillet B, Kellett DA (2012) Textures of Peritectic Crystals as guides to reactive minerals in Magmatic systems: New insights from Melting experiments. J Petrol 53:2231–2258. https://doi.org/10.1093/petrology/egs048

Gao S, Luo T-C, Zhang B-R, Zhang H-F, Han Y-W, Hu Y-K, Zhao Z-D (1998) Chemical composition of the continental crust as revealed by studies in east China. Geochim Cosmochim Acta 62:1959–1975. https://doi.org/10.1016/S0016-7037(98)00121-5

Grove TL, Holbig ES, Barr JA, Till CB, Krawczynski MJ (2013) Melts of garnet lherzolite: experiments, models and comparison to melts of pyroxenite and carbonated lherzolite. Contrib Miner Petrol 166:887–910. https://doi.org/10.1007/s00410-013-0899-9

Hirose K, Kushiro I (1993) Partial melting of dry peridotites at high pressures: determination of compositions of melts segregated from peridotite using aggregates of diamond. Earth Planet Sci Lett 114:477–489. https://doi.org/10.1016/0012-821X(93)90077-M

Holland TJB, Powell R (2003) Activity-composition relations for phases in petrological calculations: an asymmetric multicomponent formulation. Contrib Miner Petrol 145:492–501. https://doi.org/10.1007/s00410-003-0464-z

Holland TJB, Powell R (2011) An improved and extended internally-consistent thermodynamic dataset for phases of petrological interest, involving a new equation of state for solids. J Metamorph Geol 29:333–383. https://doi.org/10.1111/j.1525-1314.2010.00923.x

Holland TJB, Green ECR, Powell R (2018) Melting of peridotites through to granites: a simple thermodynamic model in the system KNCFMASHTOCr. J Petrol 9:881–900. https://doi.org/10.1093/petrology/egy048

Jean MM, Shervais JW (2017) The distribution of fluid mobile and other incompatible trace elements in orthopyroxene from mantle wedge peridotites. Chem Geol 457:118–130. https://doi.org/10.1016/j.chemgeo.2017.03.017

Keleman PB, Hirth G, Shimizu N, Spiegelman M, Dick HJ (1997) A review of melt migration processes in the adiabatically upwelling mantle beneath oceanic spreading ridges. Philosophical Trans Royal Soc A 355:283–318. https://doi.org/10.1098/rsta.1997.0010

Keleman PB, Hart SR, Bernstein S (1998) Silica enrichment in the continental upper mantle via melt/rock reaction. Earth Planet Sci Lett 164:387–406. https://doi.org/10.1016/S0012-821X(98)00233-7

Kinzler RJ (1997) Melting of mantle peridotite at pressures approaching the spinel to garnet transition: application to mid-ocean ridge basalt petrogenesis. J Phys Res 102:853–874. https://doi.org/10.1029/96JB00988

Kruger FJ (1994) The Sr-isotopic stratigraphy of the western Bushveld Complex. S Afr J Geol 97:393–398

Latypov R, Costin G, Chistyakova S, Hunt HJ, Mukherjee RA, Naldrett T (2018) Platinum-bearing chromite layers are caused by pressure reduction during magma ascent. Nat Commun 9:462. https://doi.org/10.1038/s41467-017-02773-w

Lesher CE, Spera FJ (2015) The Encyclopedia of Volcanoes. Academic Press. https://doi.org/10.1016/B978-0-12-385938-9.00005-5

Li H, Arculus RJ, Ishizuka O, Hickey-Vargas R, Yogodzinski GM, McCarthy A, Kusano Y, Brandl PA, Savov IP, Tepley FJ III, Sun W (2012) Basalt derived from highly refractory mantle sources during early Izu-Bonin-Mariana arc development. Nat Commun 12:1723. https://doi.org/10.1038/s41467-021-21980-0

Lyubetskaya T, Korenaga J (2007) Chemical composition of Earth's primitive mantle and its variance: 1. Method and results. J Phys Res 112:B3. https://doi.org/10.1029/2005JB004223

Maier WD, Barnes S-J, Groves DL (2013) The Bushveld Complex, South Africa: formation of platinum-palladium, chrome- and vanadium-rich layers via hydrodynamic sorting of a mobilized cumulate slurry in a large, relatively slowly cooling, subsiding magma chamber. Miner Deposita 48:1–56. https://doi.org/10.1007/s00126-012-0436-1

Maier WD, Barnes S-J, Karykowski BT (2016) A chilled margin of komatiite and Mg–rich basaltic andesite in the western Bushveld Complex, South Africa. Contrib Miner Petrol 171:57. https://doi.org/10.1007/s00410-016-1257-5

Mayne M, Moyen J-F, Stevens G, Kaislaniemi L (2016) Rcrust: a tool for calculating path-dependent open system processes and application to melt loss. J Metamorphic Petrol 34:663–682. https://doi.org/10.1111/jmg.12199

McKenzie D (1984) The generation and compaction of partially molten rock. J Petrol 25:713–765. https://doi.org/10.1093/petrology/25.3.713

McKenzie D, Bickle MJ (1988) The volume and composition of Melt generated by extension of the Lithosphere. J Petrol 29:625–679. https://doi.org/10.1093/petrology/29.3.625

Miller KJ, Zhu W-L, Montési LGJ, Gaetani GA (2014) Experimental quantification of permeability of partially molten mantle rock.

Earth Planet Sci Lett 388:273–282. https://doi.org/10.1016/j.epsl.2013.12.003

Naldrett AJ, Kinnaird J, Wilson A, Yudovskaya M, McQuade S, Chunnet G, Stanley C (2009) Chromite composition and PGE content of Bushveld chromitites: part 1 – the Lower and Middle groups. Appl Earth Sci 118:131–161. https://doi.org/10.1179/174327509X12550990458004

Naldrett AJ, Wilson A, Kinnaird J, Yudovskaya M, Chunnet G (2012) The origin of chromitites and related PGE mineralization in the Bushveld Complex: new mineralogical and petrological constraints. Miner Deposita 47:209–232. https://doi.org/10.1007/s00126-011-0366-3

O'Reilly SY, Griffin WL (2010) Rates of magma ascent: constraints from mantle-derived xenoliths: timescales of magmatic processes from core to atmosphere. Wiley, Oxford. https://doi.org/10.1002/9781444328509.ch6

Otto T, Stevens G, Mayne MJ, Moyen J-F (2023) Phase equilibrium modelling of partial melting in the upper mantle: a comparison between different modelling methodologies and experimental results. Lithos 444–445:107111. https://doi.org/10.1016/j.lithos.2023.107111

Pec M, Holtzman BK, Zimmerman ME, Kohlstedt DL (2017) Reaction infiltration instabilities in Mantle rocks: an experimental investigation. J Petrol 58:979–1004. https://doi.org/10.1093/petrology/egx043

Rees Jones DW, Rudge JF (2020) Fast magma ascent, revised estimates from the deglaciation of Iceland. Earth Planet Sci Lett 542:116324. https://doi.org/10.1016/j.epsl.2020.116324

Robin-Popieul CCM, Arndt NT, Chauvel C, Byerly GR, Sobolev AV, Wilson A (2012) A New Model for Barberton komatiites: deep critical melting with high Melt Retention. J Petrol 53:2191–2229. https://doi.org/10.1093/petrology/egs042

Sharpe MR, Hulbert LJ (1985) Ultramafic Sills beneath the Eastern Bushveld Complex: mobilized suspensions of early Lower Zone cumulates in a parental magma with boninitic affinities. Econ Geol 80:849–871. https://doi.org/10.2113/gsecongeo.80.4.849

Simon NSC, Carlson RW, Pearson DG, Davies GR (2007) The origin and evolution of the Kaapvaal Cratonic Lithospheric Mantle. J Petrol 48:589–625. https://doi.org/10.1093/petrology/egl074

Spiegelman M, Kenyon P (1992) The requirements for chemical disequilibrium during magma migration. Earth Planet Sci Lett 109:611–620. https://doi.org/10.1016/0012-821X(92)90119-G

Stevens G, Clemens JD, Droop GTR (1997) Melt production during granulite-facies anatexis: experimental data from "primitive" metasedimentary protoliths. Contrib Miner Petrol 128:352–370. https://doi.org/10.1007/s004100050314

Sun P, Niu Y, Guo P, Cui H, Ye L, Liu J (2018) The evolution and ascent paths of mantle xenolith-bearing magma: observations and insights from cenozoic basalts in Southeast China. Lithos 310–311:171–181. https://doi.org/10.1016/j.lithos.2018.04.015

Takahashi E (1986) Melting of dry peridotite KLB-1 up to 14 GPa: implications on the origin of peridotitic upper mantle. J Phys Res 91:9367–9382. https://doi.org/10.1029/JB091iB09p09367

Van Wijk JW, Huismans RS, ter Voorde M, Cloetingh SAPL (2001) Melt Generation at Volcanic Continental margins: no need for a Mantle Plume? Geophys Res Lett 28:3995–3998. https://doi.org/10.1029/2000GL012848

White RS (1993) Melt production rates in mantle plumes. Philosophical Trans Royal Soc Lond A 342:137–153. https://doi.org/10.1098/rsta.1993.0010

White RW, Powell R, Holland TJB, Worley BA (2000) The effect of $TiO_2$ and $Fe_2O_3$ on metapelitic assemblages at greenschist and amphibolite facies conditions: mineral equilibria calculations in the system $K_2O$–FeO–MgO–$Al_2O_3$–$SiO_2$–H2O–$TiO_2$–$Fe_2O_3$. J Metamorph Geol 18:497–512. https://doi.org/10.1046/j.1525-1314.2000.00269.x

Wilson AH (2012) A Chill sequence to the Bushveld Complex: insight into the First Stage of Emplacement and implications for the parental Magmas. J Petrol 53:1123–1168. https://doi.org/10.1093/petrology/egs011

Winter JDN (2010) Principles of Igneous and Metamorphic Petrology. Prentice Hall, New York

Yao Z, Mungall JE, Jenkins MC (2021) The Rustenburg Layered suite formed as a stack of mush with transient magma chambers. Nat Commun 12:505. https://doi.org/10.1038/s41467-020-20778-w

Zeh A, Ovtcharova M, Wilson AH, Schaltegger U (2015) The Bushveld Complex was emplaced and cooled in less than one million years - results of zirconology, and geotectonic implications. Earth Planet Sci Lett 418:103–114. https://doi.org/10.1016/j.epsl.2015.02.035

Zellmer GF, Sakamoto N, Matsuda N, Iizuka Y, Moebis A, Yurimoto H (2016) On progress and rate of the peritectic reaction fo + SiO2 → En in natural andesitic arc magmas. Geochim Cosmochim Acta 185:383–393. https://doi.org/10.1016/j.gca.2016.01.005

Zhang Y, Ni H, Chen Y (2010) Diffusion Data in Silicate melts. Rev Mineral Geochem 72:311–408. https://doi.org/10.2138/rmg.2010.72.8